ACS APPLIED MATERIALS & INTERFACES

Research Article

www.acsami.org

Adsorption and Desorption of Methylene Blue on Porous Carbon Monoliths and Nanocrystalline Cellulose

Xiaoyun He,[†] Keith B. Male,[‡] Pavel N. Nesterenko,[§] Dermot Brabazon,[†] Brett Paull,[§] and John H.T. Luong*[,‡,⊥]

[†]Irish Separation Science Cluster, Dublin City University, Glasnevin, Dublin 9, Ireland

[‡]National Research Council, Montreal, Quebec, Canada H4P2R2

[§]Australian Centre for Research on Separation Science, School of Chemistry, University of Tasmania, Hobart 7005, Australia

[⊥]Innovative Chromatography Group, Irish Separation Science Cluster, Department of Chemistry and Analytical Biological Chemistry Research Facility, University College Cork, Cork, Ireland

ABSTRACT: The dynamic batch adsorption of methylene blue (MB), a widely used and toxic dye, onto nanocrystalline cellulose (NCC) and crushed powder of carbon monolith (CM) was investigated using the pseudo-first- and -second-order kinetics. CM outperformed NCC with a maximum capacity of 127 mg/g compared to 101 mg/g for NCC. The Langmuir isotherm model was applicable for describing the binding data for MB on CM and NCC, indicating the homogeneous surface of these two materials. The Gibbs free energy of −15.22 kJ/mol estimated for CM unravelled the spontaneous nature of this adsorbent for MB, appreciably faster than the use of NCC (−4.47 kJ/mol). Both pH and temperature exhibited only a modest effect on the adsorption of MB onto CM. The desorption of MB from CM using acetonitrile was very effective with more than 94 % of MB desorbed from CM within 10 min to allow the reusability of this porous carbon material. In contrast, acetonitrile was less effective than ethanol in desorbing MB from NCC. The two solvents were incapable of completely desorbing MB on commercial granular coal-derived activated carbon.

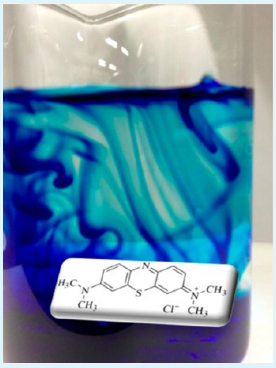

KEYWORDS: *carbon monolith, nanocrystalline cellulose, activated carbon, methylene blue, adsorption, desorption, kinetics*

INTRODUCTION

Porous carbon materials have attracted significant attention[1−3] for diversified applications including pollutant removal/remediation, because of their high specific surface area, high porosity, adsorption capacity, and excellent thermal/chemical stability. Among various fabrication procedures of carbon monoliths, of interest is the pyrolysis of a carbon rod produced from the polymerization of a resorcinol−formaldehyde copolymer on silica particle templates with iron serving as the catalyst for localized carbonization.[4,5] The resulting polymer can be doped with a metallic salt, in turn forming encapsulated metallic nanoparticles during the course of carbonization. Such nanoparticles play an important role in the conversion of a fraction of amorphous carbon into graphitic domains and are removable from carbon monoliths by chemical/acid etching.

In brief, over 100 000 types of dyes have been used for industrial applications in textile, pulp and paper, pharmaceuticals, tannery, etc.[6] Dyes used in the textile industry must have a high chemical and photolytic stability; therefore, biodegradation or biological treatment of such dyes is very difficult, time-consuming, and ineffective. Currently, the textile industry uses more than 10 000 different dyes with an annual consumption of 7×10^5 tons and their eventual discharge into waste streams poses a serious environmental problem.[7] Even if they are degraded, their degradation products are still toxic, carcinogenic, and teratogenic for living organisms.[8] Besides the undesirable color, their breakdown products also exhibit a mutagenic or carcinogenic effect on human beings and their ingestion can cause severe damage to organisms. Several methods have been attempted to remove or remediate dye-contaminated wastes and adsorption is a low-cost and effective method for the removal of dyes from aqueous solutions. Various organic and inorganic adsorbents including modified graphite powder and emerging carbon nanotubes have been attempted for the removal of organic dyes from aqueous waste waters. However, such adsorbents usually suffer from difficulties in the regeneration and separation from the waste stream. In particular, activated carbon with high surface areas (700−1500 m^2/g) is highly effective for the removal of dyes, pigments, and other inorganic/organic pollutants. However, activated carbon regeneration typically involves drying at elevated temperature, i.e., it is costly and causes partial destruction of this material.

As an important basic dye used for printing calico, dyeing cotton and leather, methylene blue (MB) could cause various harmful effects such as eye burns, irritation to the gastrointestinal tract and to the skin.[9] The article describes the applicability of powdered monolithic carbon for the removal of

Received: July 5, 2013
Accepted: August 9, 2013
Published: August 9, 2013

   dx.doi.org/10.1021/am403222u | ACS Appl. Mater. Interfaces 2013, 5, 8796−8804

MB from solution. Porous CM was synthesized and characterized to study the adsorption-desorption kinetics and equilibrium isotherms for MB. Carbon monoliths have been used as the stationary phase for HPLC[10,11] or electrode materials.[12] To the best of our knowledge, this study is the first demonstration for the use of CM to remove this toxic dye and unravel an effective procedure for its regeneration. The binding capacity and kinetics of this carbon material are also compared with that of nanocrystalline cellulose[13] (NCC), a rod-shaped renewable nanomaterial with exceptional strength and physicochemical properties that can be prepared from inexpensive renewable biomass. NCC is virtually nontoxic and poses no serious environmental concerns, providing impetus for its use in waste water treatment. Although NCC has been developed for a plethora of diversified applications, its applicability as an effective reusable adsorbent for the removal of organic pollutants, dyes, etc. has not been demonstrated. For comparison, commercial activated carbon is also included in this study.

MATERIALS AND METHODS

Carbon monolith (CM) was prepared using the same grade of silica gel as the template. More detailed information on the fabrication of CM can be found elsewhere.[10−12] Granular coal-based activated carbon (AquaSorb 2000) was obtained from Jacobi Carbons (Birkenhead, UK). This activated carbon material has a surface area of 1100 m^2/g (BET, N_2). The NCC used in this study was produced by hydrolysis of microcrystalline cellulose (MCC, Sigma) in 1 M ammonium persulfate, APS, (FMC Industrial Chemicals, Philadelphia, PA) as previously reported by our group.[13,14] The starting biomass material MCC (10 g) was added to 1 L of 1M APS solution (conductivity ~230 mS/cm). The suspension was heated to 60 °C for 16 h, resulting in a white NCC suspension. After centrifugation at 12 000 rpm, RCF = 22 100 for 10 min, the supernatant was decanted, and 1 L of water was added to the NCC pellet, followed by 5 min of vigorous mixing and repeated centrifugation. After 4−5 repeated centrifugation/washing cycles, the solution conductivity approached that of deionized water, ~5 μS/cm (pH ~5). The final pellet was reconstituted in 100 mL of deionized water and lyophilized to yield a white powder.

Instrumentation and Characterization. High-resolution scanning electron microscopy (SEM) micrographs of the prepared monolithic materials were obtained using a field-emission Hitachi S-5500 (FE-SEM) (Dallas, TX) at an accelerating voltage of 10−20 kV. High-resolution imaging for such carbon materials was also performed by using a JOEL JEM-2100 LaB_6 transmission electron microscope (TEM) (Tokyo, Japan) operated at 200 kV. The samples for TEM measurements were suspended in 2-propanol and dropped onto holey carbon-coated copper grids. For NCC imaging, low-voltage transmission electron micrographs were obtained by a Delong LVEM (Soquelec, Montreal, QC, Canada) low-voltage TEM operating at 5 kV. A small amount of NCC material (10 mg) was suspended in water (10 mL) and sonicated to disperse the material. A 4 μL drop of well-dispersed suspension was then dried on a Formvar-carbon-coated grid and analyzed. Measurements were made using QCapture Pro Version 6.0 software and statistical analysis was performed using GraphPad InStat Version 3.06 software. Atomic force microscopy (AFM) micrographs of the prepared NCC were obtained using a Nanoscope IV (Digital Instruments, Veeco, Santa Barbara, CA) with a silicon tip operated in tapping mode with a silicon cantilever (MPP-11100, spring constant ~40 N/m, resonance frequency ~300 kHz, NanoDevices, CA) at scan rates of 0.5 Hz with 512 × 512 pixels.

A Micromeritics TriStar II 3020 surface area analyzer, (Norcross, GA) was used to measure the specific surface area and the pore volume using the nitrogen adsorption/desorption technique. The Raman spectrum was obtained on a Horiba Jobin Yvon LabRam800HR with a CCD detector (Edison, NJ). The argon ion laser used is the Innova 70-C-2 made by Coherent (Santa Clara, CA). The laser power was 6 mW with excitation wavelength 514.5 nm. A magnification of ×50 on the objective lens was used to focus the laser beam and collect backscattering radiation. The exposure time of all spectra recorded was 10 s and each spectrum was the accumulation of three scans. Thermogravimetric analysis (TGA) was conducted with an Netzsch STA 449F1 (Netzsch Instruments, Burlington, MA, USA) at a heating rate of 10 °C/min from room temperature to 600 °C under helium purge gas.

Adsorption Kinetics of Methylene Blue (MB). The adsorption capacity of MB on the adsorbent is calculated as $q = V(C_o - C_t)/m$, where V is the solution volume, C_o is the initial MB concentration, C_t is the MB concentration in the solution at a given time (t), and m is the adsorbent mass. The dye used was purchased from Sigma-Aldrich with a molecular weight ~320 g/mol, corresponding to anhydrous methylene blue. All containers used for methylene blue solutions were of polypropylene to minimize the dye adsorption. The adsorption kinetics was investigated using the pseudo-first-order and pseudo-second-order models. The concentration of active sites on the surface of the adsorbent greatly outnumbers the MB concentration, i.e., only the dye concentration significantly affects the adsorption rate, so the reaction behaves more like a first- or second-order reaction (pseudo).

For each initial dye concentration (C_o), the amounts of MB adsorbed at a given time, q_t, can be related to C_t as shown in Table 1.

Table 1. Pseudo-First-Order and Pseudo-Second-Order Adsorption Kinetics

pseudo-first-order kinetics	$\frac{dC}{dt} = -k_1 C$ or $C = C_o e^{-k_1 t}$ (1)
	where k_1 (min^{-1}) = the rate constant
	q_t= the amounts of dye adsorbed at a given time
	$q_t = q_e(1 - e^{-k_1 t})$ (2)
	where $q_e = VC_o/m$, the amount of dye adsorbed at equilibrium
	C_o = initial concentration of MB
	m = amount of the adsorbent
	V = volume of the MB solution
pseudo-second-order kinetics	$\frac{dC}{dt} = -k_1 C^2$ or $\frac{1}{C} - \frac{1}{C_o} = k_1 t$ (3)
	$q_t = \frac{q_e C_o k_1 t}{1 + C_o k_1 t} = \frac{q_e^2 k_2 t}{1 + q_e k_2 t}$ (4)
	$k_2 = (m/V)k_1$

Nonlinear regression analysis was then applied to estimate the values for $q_e = V(C_o - C_e)/m$, k_1, and k_2. A plot of q_e vs. C_e, the residual concentration in the solution, was then performed to validate the applicability of the Langmuir isotherm equation, $q_e = q_{max}K_L C_e/(1 + K_L C_e)$ where q_{max} is the Langmuir constant related to maximum adsorption capacity and K_L is the Langmuir constant related to binding energy of the adsorption system as discussed later. The q_{max} value was then used for the estimation of the specific surface area (SSA) of CM and NCC as $(q_{max}/MW)\alpha_{MB}N_{Avo}$, where MW is the molecular weight of MB, α_{MB} is the occupied surface area of one MB molecule (~1.3 nm^2, assuming the MB molecule is lying flat on the adsorbent surface, 17.0 × 7.6−130 $Å^2$) and N_{Avo} is the Avogadro number (6.023×10^{23} mol^{-1}).

A calibration curve was established for MB absorbance at 660 nm ($Abs_{660\ nm}$) vs MB concentration [MB], providing a straight line (up to 20 μM) with a slope of 0.062 $Abs_{660\ nm}/\mu M$ [MB]. Aqueous solutions (12 mL) containing different concentrations of MB (100-1500 μM, diluted from a 4 mM stock solution in 20 mM phosphate buffer, pH 7.5), were added to ground samples (12 mg) of CM and NCC and rotated or stirred in the case of NCC for up to 40 min. Samples with AC were rotated with MB for a longer time period of up to 3 h. Small samples (~ 300 μL) were taken every 30 s for the first 3 min and then

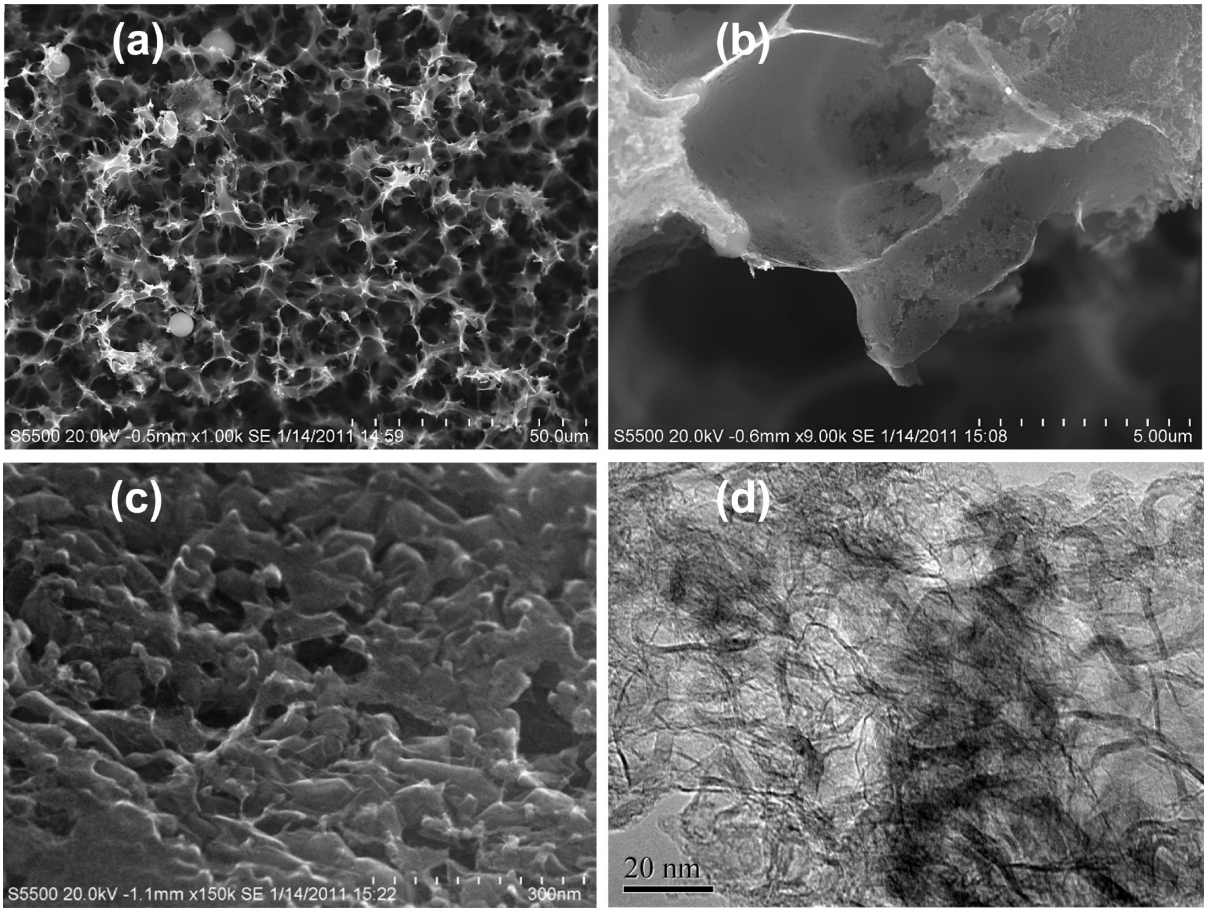

Figure 1. FE-SEM images of (a) macroporous networks, (b) macroporous walls, (c) mesoporous structure of CM; and (d) TEM image of CM.

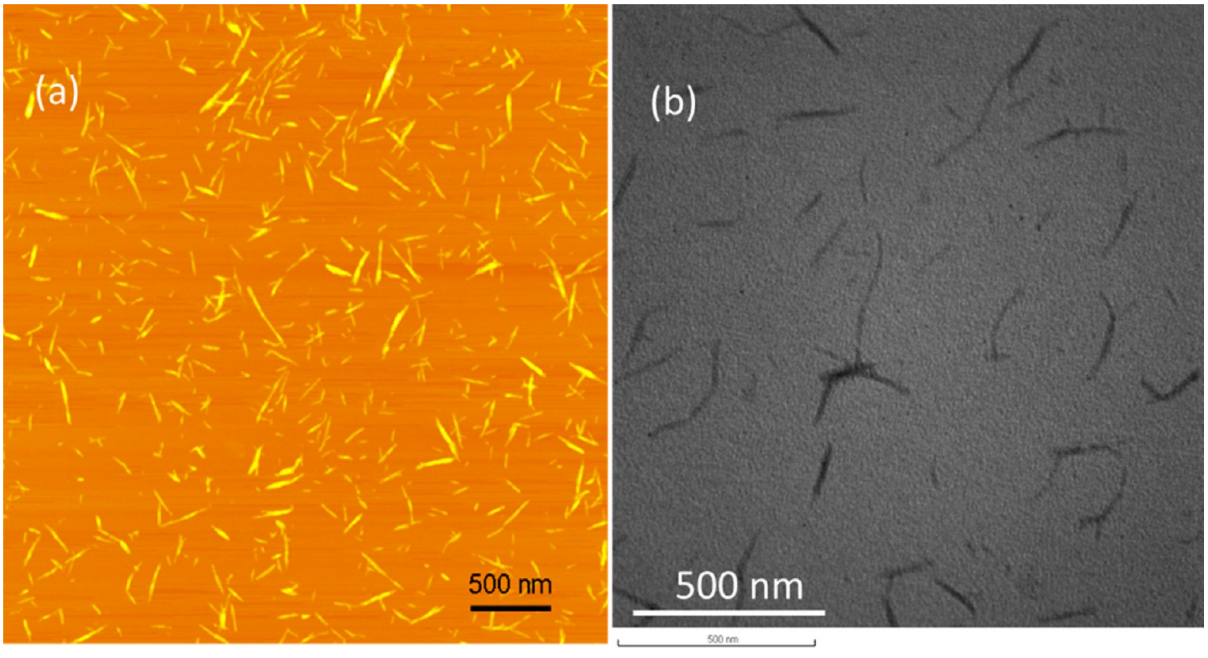

Figure 2. (a) AFM and (b) TEM images of NCC.

at 4, 5, 10, 15, 20, and 40 min and up to 3 h for AC. These samples were immediately centrifuged at 12 000 rpm and the supernatants (after centrifugation) were tested (diluted 10−100× depending on the concentration of MB) for the residual concentration of MB left in solution, following any MB binding to the adsorbents, and compared to the starting concentration. From the calibration curve of MB, the amount of MB bound (mg) was then calculated and the MB adsorption in mg/g of sample was determined. Unless otherwise indicated, the binding experiments were performed at ambient temperature, 22 ± 1 °C and neutral pH. For the Langmuir isotherm

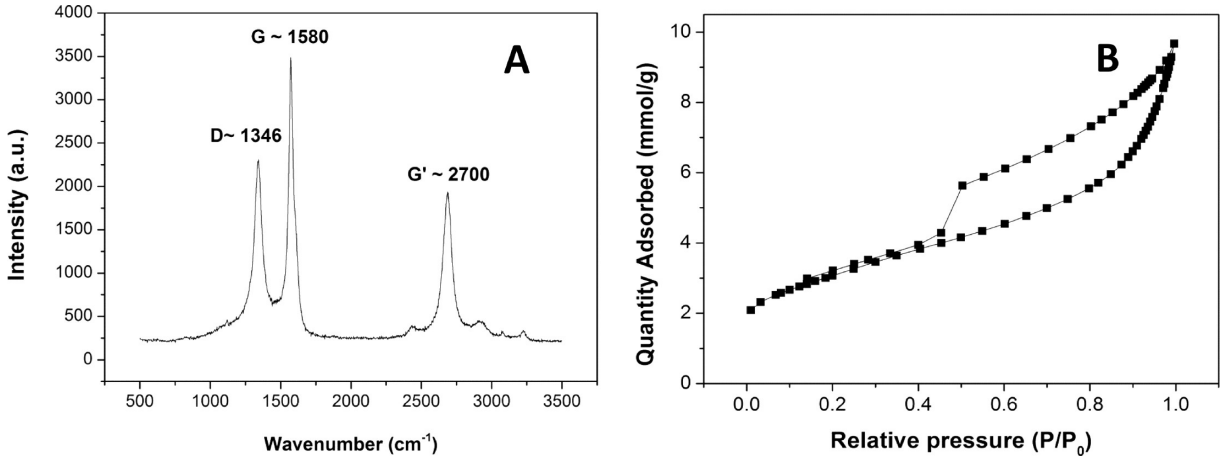

Figure 3. (A) Raman spectrum of CM. (B) Nitrogen adsorption/desorption isotherms of CM.

plots extra q_e vs C_e points (in addition to those calculated from the adsorption isotherms) were determined by the addition of different concentrations of MB to the adsorbents for 16 h (i.e. end point determination).

Desorption of Methylene Blue (MB). Desorption of MB from AC, CM, and NCC was performed using ethanol or acetonitrile. In this serial desorption experiment, MB containing ethanol or acetonitrile was removed by centrifugation and fresh ethanol or acetonitrile was added every 2 min to prevent the readsorption of MB onto the absorbent.

RESULTS AND DISCUSSION

Characteristics of Carbon Monolith (CM) and Nanocrystalline Cellulose (NCC). The CM skeleton was constructed by a series of mesopores with irregular shapes except for a few micropores on the walls. The inner pore surfaces of the CM sample were considerably smooth in texture (Figure 1a–d), similar to materials reported in the literature.[11,12] The CM sample also exhibited a higher degree of graphitization as attested by the presence of a high density of graphite ribbons. The carbon content was 86±3 wt % for CM and the oxygen content was 10 ± 2 wt % as estimated by energy-dispersive X-ray spectroscopy. Atomic force microscopy (AFM) and transmission electron microscopy micrographs confirmed the production of highly uniform NCC (Figure 2a, b). NCC was stable to ~220–270 °C with <5% mass loss below this temperature (T_{d5}). The use of APS resulted in the formation of highly carboxylated NCC, as opposed to sulfonated NCC produced using mineral acids. The resulting NCC exhibited a degree of oxidation of 0.10, and average dimensions of 130 nm in length and 6–7 nm in width. Other characteristics of this material including NMR, FTIR signatures, crystallinity index, and the crystal structure can be found elsewhere.[10]

Raman Spectroscopy and BET Measurement. On the basis of the pioneering work of Tuinstra et al.,[15] the Raman spectrum for CM was acquired and compared to that of commercial graphite. CM exhibited three major Raman peaks, as commonly observed for carbon nanotubes and other carbon materials, i.e., the sp^3 and sp^2 carbon phases coexisting in the sample (Figure 3A). The disordered *D*-band at ~1350 cm^{-1} is Raman active, reflecting the imperfection or loss of hexagonal symmetry in the carbon structure.[16] The *G* (graphite) band, common to all sp^2 carbon materials, at ~1580 cm^{-1}, corresponds to the Raman active $2E_{2g}$ mode of a two-dimensional network structure, i.e., the C–C bond stretching, in all carbon and graphitic materials.[16] Previous studies have revealed that the intensity ratio of the D to the G band, *R*, ($R = I_D/I_G$) was inversely proportional to the in-plane crystallite sizes (L_a).[15,17] The estimated *R* value of CM was 0.64, compared with 0.14 for commercial graphite.

The nitrogen adsorption/desorption isotherm of CM exhibited type IV isotherms,[18] a typical signature of materials consisting of both mesopores and micropores (Figure 3B). The hysteresis loops were type B, as reflected by a steep slope in the region close to the saturation pressure and a steep slope for desorption at mid-range pressures. Materials with cylindrical pores with bottle-shape structures (wide openings and narrow "necks") or slit-type pores have been known to display such hysteresis.[19] There was no ordered structure or narrow pore size distribution within this mesoporous carbon material as exemplified by the absence of a sharp condensation/evaporation step, or a pronounced hysteresis loop (type H1). Considering capillary condensation for both materials starting at $P/P_o \approx 0.45$, their skeleton pores should be mainly composed of mesopores, in agreement with the estimated pore diameter of 10.7 nm for CM using the Barrett–Joyner–Halenda method.[20] The first plateau of the isotherm was observed at relatively low P/P_o values (~0.15), indicating the presence of some microporous structures (Figure 3B). The total micropore volume derived from the *t*-plot was 0.016 cm^3 g^{-1} (average, $n = 3$). The average BET specific surface area ($n = 3$), evaluated at P/P_o from 0.05 to 0.25, was 272 ± 32 m^2/g with a total core volume of 0.42 cm^3/g.

Table 2. Structural Characteristics of CM ($n = 3$)

S_{BET} [a] (m^2 g^{-1})	V_{total} [a] (cm^3 g^{-1})	D_{meso} [b] (nm)	V_{micro} [c] (cm^3 g^{-1})
272 ± 32	0.42 ± 0.08	6.54 ± 0.68	0.016 ± 0.004

[a]The Brunauer–Emmett–Teller (BET) method was used to calculate the specific surface areas. [b]The Barett–Joyner–Halenda method was used to calculate mesopore diameter from the adsorption branches of the isotherms. [c]Micropore volumes were calculated by the *t*-plot.

Adsorption Kinetics of Methylene Blue (MB). A series of experiments was conducted to study the adsorption kinetics of MB on CM, AC, and NCC. The plots of q_t versus time (t) for various initial concentrations of MB on such adsorbents are shown in Figure 4. The adsorption capacity of CM increased and reached equilibrium within 5 min, whereas over 10 min of

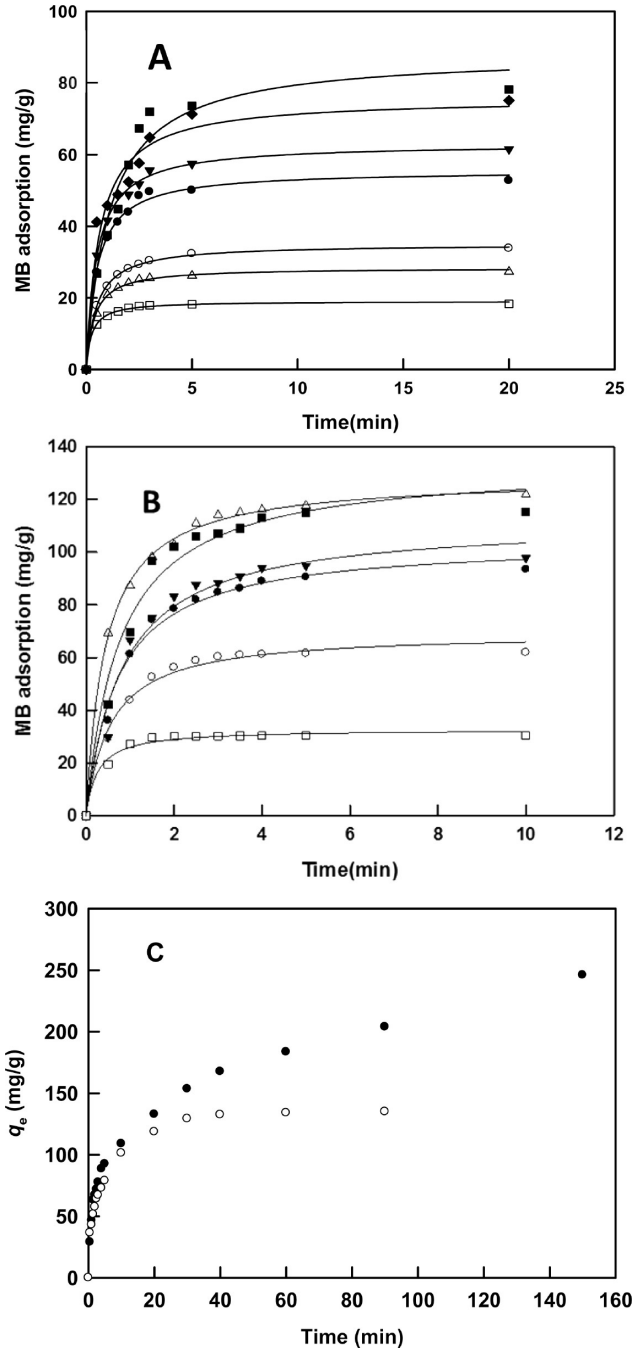

Figure 4. Adsorption kinetics at different concentrations (μM) of methylene blue (MB): (A) on NCC, bottom to top, 102, 170, 201, 411, 590, 1003, and 1454 ; (B) on CM, bottom to top: 96, 196, 302, 386, 776, and 1150; and (C) on AC, bottom to top, 424 and 1221. The solid lines were obtained by fitting the data using the pseudo-second-order kinetics.

contact time was required for the q_t value of NCC to reach the plateau, particularly at high initial MB concentrations. For NCC, the pseudo-second-order model was more applicable for describing the adsorption data as attested by the higher correlation of coefficient (R^2), compared to the first-order-kinetics (Table 3). However, the adsorption of MB onto CM could be well-represented by the first-order or second-order model (Table 3).

CM exhibited a high degree of graphitization and its inner pore surfaces appeared considerably smooth in texture. The presence of oxygen was expected to promote hydrogen bonding interaction between MB and the absorbent, which in turn favored the binding of MB onto CM.

In contrast, the adsorption of MB to AC was much slower and the contact time required for the q_t value of AC to reach the plateau was several hours particularly at high initial MB concentrations. It should be noted that the binding capacity for MB on AC was higher than on CM or NCC, confirming a very high surface area (1100 m^2/g) and a very high MB binding (280 mg/g) of this carbon material as indicated by the manufacturer (AquaSorb 2000, Birkenhead, U.K.).[21]

Langmuir Adsorption Isotherms. The Langmuir adsorption isotherm was then applied to describe the adsorption process by plotting q_e vs C_e, the equilibrium or residual concentration of MB in the solution. This adsorption isotherm with some rational basis assumes that the adsorbent surface consists of active sites with uniform energy for the formation of a monolayer.[22] The Langmuir constant is also related to the Gibbs free energy (ΔG^o) of sorption reaction as $\Delta G^o = -RT\ln K_L$, where T= absolute temperature (295 K) and R (the gas constant) = 8.314 J mol^{-1} K^{-1}. The negative value of the free energy indicates the feasibility of the process and the spontaneous nature of the adsorption. At low adsorbate concentrations ($K_LC_e \ll 1$), the Langmuir model becomes a linear isotherm ($q_e = q_{max}K_LC_e$) and follows Henry's law. Alternatively, at high adsorbate concentrations ($1 + K_LC_e \approx K_LC_e$), it predicts a constant monolayer sorption capacity, i.e., $q_e = q_{max}$. Nonlinear regression analysis was performed to estimate the Langmuir constants because the linearization of the Langmuir model tends to fit experimental data better at higher concentrations[23] and might violate the error variance and normality assumptions of standard least squares.[24] Other modified Langmuir models such as Radke–Prausnitz isotherm[25] and Langmuir–Freundlich (Sips equation)[26] were not attempted in this study because they involve more than two fitting parameters with no physical meaning or rational basis.

The Langmuir isotherm model (Figure 5) appeared to well-represent the binding data for MB on NCC and CM judging from the obtained correlation coefficients R^2 (Table 4), indicating the homogeneous nature of CM and NCC. CM outperformed NCC with respect to the amount of MB loading (127.53 vs 101.16 mg/g), faster binding kinetics and its affinity to MB binding, as reflected by a higher q_{max} and a very steep initial slope of the isotherm. It should be noted that $C_e^* = 1/K_L$, the equilibrium concentration at which the loading is 50% of the maximum capacity, was estimated to be 2.02 and 162.3 μM, respectively for CM and NCC. The Gibbs free energy ($\Delta G^o = -RT\ln K_L$) was estimated at −15.22 and −4.47 kJ/mol for CM and NCC, respectively, to confirm the spontaneous nature of the adsorption of CM for this dye (Table 4).

Thus, one could use CM to saturate this adsorbent with MB at both low and high concentrations, corresponding to very low residual MB in the solution. This was an important finding since the regulatory authorities always desire to limit the maximum concentration of a pollutant such as organics, metals, etc. For comparison, the binding of MB on *Polyalthia longifolia* (Ashoka) seed powder is time-consuming,[26] more than 60 min, and the binding capacity of this material for MB is below 10 mg/g. The q_{max} values of CM and NCC were compared favorably with those obtained for activated carbon prepared from different sources, ranging from a few mg/g to hundreds of mg/g. Notably, the monolayer sorption capacity of activated carbon prepared from pea shell for MB is as high as 246.9 mg/

Table 3. Estimated Kinetic Parameters of the Two Adsorption Isotherms for Methylene Blue (MB)

(A)

NCC	eq	param	methylene blue concentration (μM) 102	170	201	411	590	1003	1454
pseudo-second order	$q_t = q_e(1 - e^{-k_1 t})$	q_e	17.7	25.9	31.5	50.2	56.7	68.4	78.4
		k_1	2.18	1.66	1.36	1.30	1.34	1.04	0.68
		R^2	0.904	0.953	0.917	0.948	0.894	0.664	0.969
pseudo-second order	$q_e = (q_e^2 k_2 t)/(1 + q_e k_2 t)$	q_e	19.1	28.4	35.0	55.6	63.1	75.7	88.2
		k_2	0.2084	0.0934	0.0584	0.0360	0.0317	0.0211	0.0103
		R^2	0.998	0.998	0.999	0.994	0.997	0.965	0.967

(B)

CM			methylene blue concentration (μM) 96	196	302	386	776	1150
pseudo-first order	$q_t = q_e(1 - e^{-k_1 t})$	q_e	30.4	61.6	90.2	95.7	115	115
		k_1	2.13	1.26	1.07	0.99	1.49	1.01
		R^2	0.999	0.999	0.996	0.988	0.984	0.993
pseudo-second order	$q_e = (q_e^2 k_2 t)/(1 + q_e k_2 t)$	q_e	32.7	69.6	84.3	112	131	129
		k_2	0.119	0.0256	0.0127	0.0109	0.0096	0.0174
		R^2	0.985	0.988	0.990	0.974	0.975	0.998

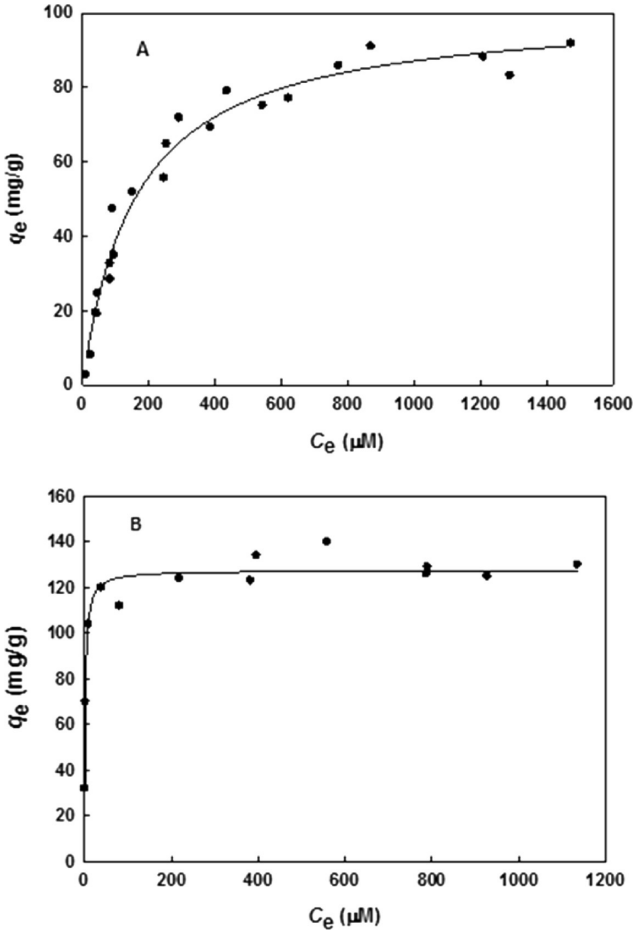

Figure 5. Lamgmuir adsorption isotherm of methylene blue on (A) NCC and (B) CM.

g. However, the equilibrium time is 40 and 100 min at concentrations of 100 and 150 mg/L, respectively, and 180 min for higher concentrations (200, 250, 300, and 350 mg/L).[27] Similarly, in this study the value of q_{max} for the granular coal based activated carbon (AquaSorb 2000) approached 300 mg/g, but the equilibrium time was in the order of hours at 384 mg/L.

Table 4. Estimated Adsorption Parameters of Langmuir Isotherms at Room Temperature[a]

Langmuir adsorption model	NCC	CM
$q_e = \frac{q_{max} K_L C_e}{1 + K_L C_e}$	q_{max}= 101.16 mg/g (SE = 3.07)	q_{max}= 127.53 mg/g (SE = 2.11)
	K_L = 0.0062 μM^{-1} (SE = 0.0006)	K_L = 0.496 μM^{-1} (SE = 0.082)
	R^2 = 0.974	R^2 = 0.957
	ΔG^o = −4.47 kJ/mol	ΔG^o = −15.22 kJ/mol

[a]SE, standard error; ΔG^o (Gibbs free energy) = $-RT\ln K_L$, where T = absolute temperature (295 K), R (the gas constant) = 8.314 J mol^{-1} K^{-1}.

As a rectangular volume of dimensions 1.7 × 0.76 × 0.325 nm,[28−31] the projected area of MB has been given as 1.35, 1.32, and 1.30 nm^2, and in this work will be taken as 1.30 nm^2. Thus, it is very unlikely that MB is able to fill in micropores of the adsorbent (< 2 nm) and the sorption should occur in mesopores and macropores. Nevertheless, the two $-N(CH_3)_2$ groups of this dye should be able to protrude into such micropores to display hydrophobic interaction and hydrogen bonding with the walls of such micropores. In macropores and mesopores, the sorption depends not only upon the fluid wall attraction but also on the attractive interactions between the MB molecules, leading to possible multilayer adsorption.

On the basis of the q_{max} estimated from the Langmuir model for CM and NCC (Table 4), a surface area of 312 and 248 m^2/g was estimated for CM and NCC. The surface area estimated by BET (272 ± 32 m^2/g) was in agreement with the MB adsorption procedure for CM (312 m^2/g). Considering NCC as a cylinder with a length of 130 nm, a diameter of 6−7 nm, and a density of 1.6 g/cm^3, the specific surface area (SSA) of NCC should be 426 and 367 m^2/g, respectively. SSA for 1 g of NCC is estimated as NS_a, where S_a is the surface area of one NCC molecule or $2\pi(\text{radius})^2 + 2\pi(\text{radius})(\text{length})$. The number ($N$) of NCC molecules per gram is estimated as V_T/V_s, where V_s is the volume of one NCC molecule or 2π-

dx.doi.org/10.1021/am403222u | ACS Appl. Mater. Interfaces 2013, 5, 8796−8804

(radius)^2(length) and V_T is the volume for 1 g of NCC = 1/density.

Of interest was the comparison of the performance of NCC and CM obtained in this study versus some cellulose-based materials reported in the literature. Spent mushroom substrate, a renewable biowaste was used as an adsorbent to remove MB from aqueous solution.[32] The adsorption kinetics is governed by the pseudo-second-order model with a maximum adsorption capacity of 63.5 mg/g at 303 K. The equilibrium time ranges from 25−100 min and is dependent on the initial MB concentration. A review paper of Sharma et al.[33] presents activated carbon derived from various natural or agricultural wastes which have been used as dye adsorbents with their adsorption capacity ranging from 2−600 mg/g. Foo and Hameed[34] also provide an overview of dye removal via activated carbon adsorption process. Numerous publications concerning biomass-derived substrates and their adsorption capacity for different classes of dyestuffs from dilute aqueous solutions have been described in the literature.[35,36]

The intraparticle diffusion model[37] can be expressed as $q_t = x + K_p t^{1/2}$, where t is the contact time, x is the boundary layer thickness, and K_p is the intraparticle diffusion rate constant. The plot q_t vs $t^{1/2}$ for CM and NCC at different MB concentrations displayed multilinearity (figure not shown), indicating that besides intraparticle diffusion other processes were also involved in the rate controlling step. Initially, sharp linear curves showed rapid transport of adsorptive molecules from the bulk solution to the adsorbent surface. The adsorbate was then subject to internal diffusion, where it was transferred to the interior of the adsorbent by the diffusion of the adsorbate molecules through macropores, wider and smaller mesopores, and micropores.[38] The gradual adsorption showed by the second linear portion confirmed that intraparticle diffusion was the rate-limiting step.[39] Finally, the equilibrium was reached due to the saturation of the binding sites and/or extremely low MB concentration in the solution. The curves did not pass through the origin, again confirming more than one step involved in the adsorption process.[40]

Effects of pH and Temperature. On the basis of binding kinetics and binding capacity, CM was chosen for further investigation with respect to pH and temperature effects as well as its plausible regeneration. The sorption capacity was identical at three different pHs: 4.5 (20 mM sodium acetate), 7.5, and 10.5 (20 mM sodium borate), indicating no noticeable charge interaction between MB and CM (Figure 6A). Such results were not completely unexpected since the MB surface with pK_a of 3.8 was predominantly neutral and did not participate in ionic/electrostatic interaction with hydrophobic and neutral CM. Thus, CM adsorbed MB mainly via hydrophobic interaction, $\pi-\pi$ stacking and hydrogen bonding.

As described earlier, kinetics of MB onto CM followed the pseudo-second-order model, implying that the rate-limiting step might be chemisorption.[41] The adsorption capacity of CM slightly increased with the increase of adsorption temperature to 60 °C (Figure 6B). Considering the apparent activation energy of MB adsorption on CM using the Arrhenius equation

$$k_2 = k_o e^{-E_a/RT}$$

where k_2 is the pseudo-second-order rate constant defined in Table 1, k_o is the temperature-dependent factor, E_a is the apparent activation energy of the adsorption, R is the gas constant, and T is the adsorption absolute temperature. The activation energy was estimated to be 18.52 kJ/mol, compared

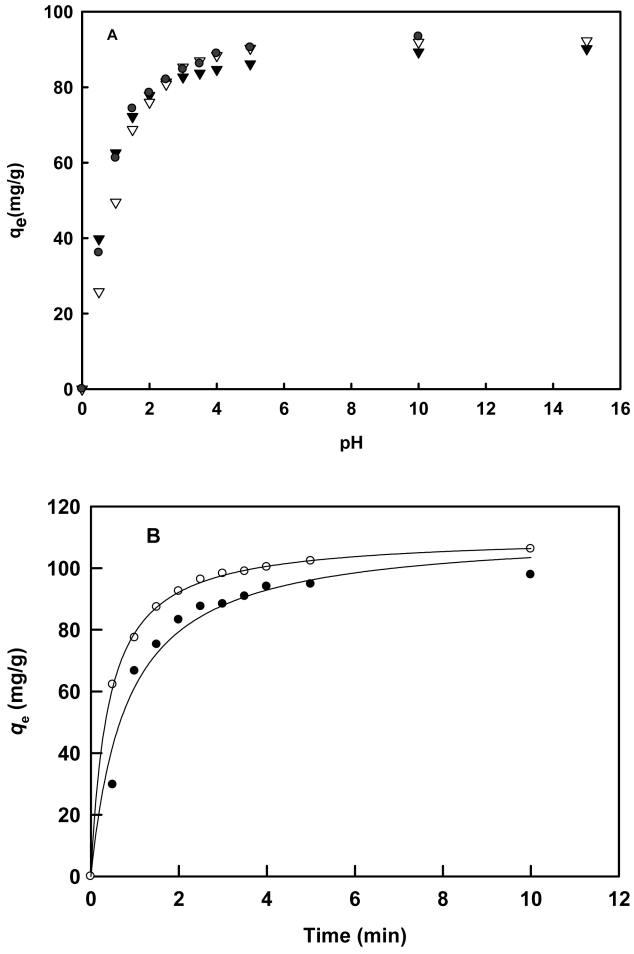

Figure 6. (A) pH effect on the binding kinetics of methylene blue (MB) on CM at three different pHs: (▼) pH 4.5, (●) pH 7.5, and (▽) pH 10.5. (B) The temperature effect on the binding kinetics of methylene blue on CM: 25 °C (lower curve), and 60 °C (upper curve).

to 27.63 kJ/mol for the adsorption of MB onto bamboo charcoal.[42] Notice also that the contact time of MB adsorbed onto bamboo charcoal requires several hours to reach equilibrium. Apparently, increasing temperature decreased the solution viscosity, leading to an enhanced diffusion rate of adsorptive molecules across the external boundary layer and in the internal pores. From a practical viewpoint, the adsorption of MB on CM should be carried out at room temperature and neutral pH.

The desorption using 1 M KOH or nitric acid as described for the desorption of MB onto activated carbon was not effective,[43] thus, this approach was not considered in this study. The desorption of MB adhered on CM by ethanol was rapid at room temperature, however, only 50% of MB was desorbed and increasing desorption temperature up to 60 °C did not accelerate the desorption process (Figure 7A). Apparently, ethanol was only capable of effecting the desorption of MB adhered on the CM surface, not in the macro and mesopores. Finally, desorption of MB adhered on CM by acetonitrile using the above protocol even at room temperature was most effective, with ∼95% of the MB desorbed in the first 10 min. Such a result confirmed that acetonitrile could remove the MB from the surface, macro and mesopores. In contrast, the desorption of MB from AC was not very effective as only 42

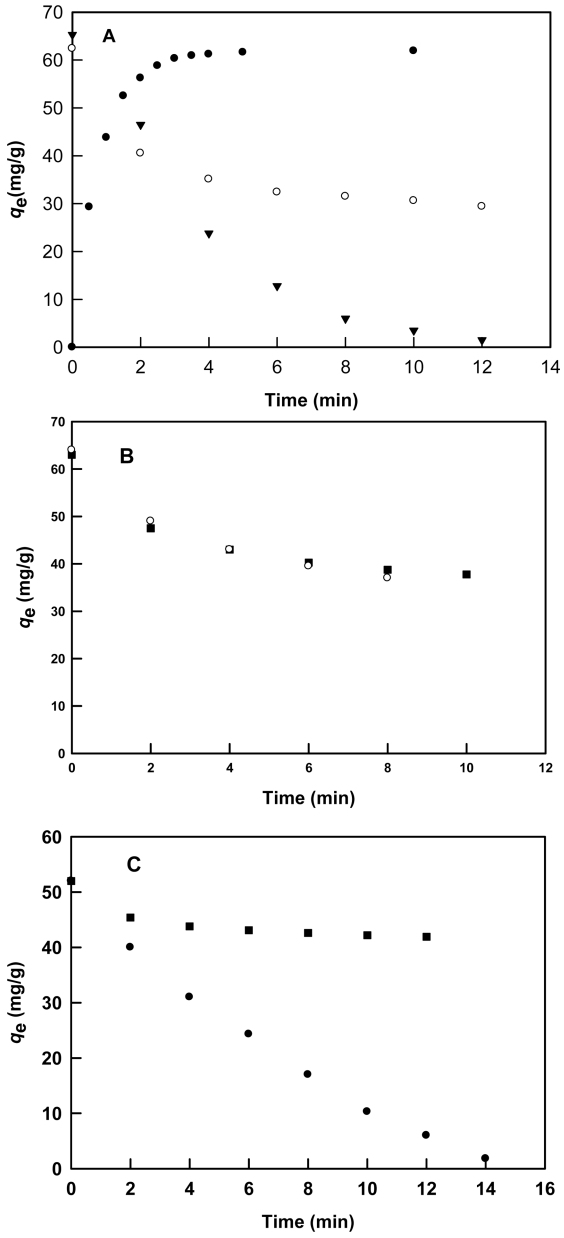

Figure 7. (A) Time course for the desorption of 4 mL methylene blue (MB 200 μM) adsorbed on CM (4 mg) by ethanol (○) and acetonitrile (▼).The time course for the adsorption of 4 mL of methylene blue (MB 200 μM) adsorbed on CM (4 mg) (●). (B) Time course for the desorption of 4 mL of methylene blue (MB 200 μM) adsorbed on AC (4 mg) by ethanol (○) and acetonitrile (■). (C) The time course for the desorption of 4 mL of methylene blue (MB 800 μM) adsorbed on NCC (4 mg) by ethanol (●) and acetonitrile (■).

and 40 % of MB was desorbed with ethanol and acetonitrile, respectively (Figure 7B). It should be note that activated carbon regeneration typically involves drying the carbon followed by heat treatment at 500−900 °C. This procedure is costly and causes partial cracking and charring of the activated carbon, resulting in up to a 20% loss of adsorptive capacity due to a decrease in surface area.[44] In comparison, the desorption of MB from NCC using acetonitrile was not very effective as only 18% of MB was desorbed. However, the desorption with ethanol was much more effective with more than 90% removal after 7 desorption cycles (Figure 7C).

CONCLUSION

In brief, we have demonstrated the application of powdered porous carbon monolith and nanocrystalline cellulose with high surface areas for the adsorption of methylene blue. In particular, carbon monoliths with a high specific surface area, high mesopore volume, and narrow size distributed mesopores can be designed in any dimension and shape to facilitate their reusability without tedious separation from the treated waste stream such as experienced with activated carbon powder. The test model, methylene blue with a molecular weight of 320 was adsorbed and easily desorbed from CM and NCC. Such results attested the potential use of these promising materials, which can be easily prepared from inexpensive and abundant materials for the removal of recalcitrant contaminants in water and waste waters. Magnetic nanoparticles[45] and/or TiO_2[46] can be readily prepared and incorporated into carbon monoliths via adsorption to facilitate the process design and perform both adsorption and photocatalytic remediation of this blue dye as well as other organic pollutants.

AUTHOR INFORMATION

Corresponding Author

*E-mail: john.luong@cnrc-nrc.gc.ca or j.luong@ucc.ie.

Notes

The authors declare no competing financial interest.

ACKNOWLEDGMENTS

The authors thank Science Foundation Ireland (Grant 08/SRC/B1412) for research funding under the Strategic Research Cluster program and (Grant 03/IN.3/1361/EC07) for FE-SEM imaging. Silica gel was a gift from Prof. Peter Myers, University of Liverpool, U.K.

REFERENCES

(1) Lee, J.; Kim, J.; Hyeon, T. *Adv. Mater.* **2006**, *18*, 2073−2094.
(2) Liang, C.; Li, Z.; Dai, S. *Angew. Chem., Int. Ed.* **2008**, *47*, 3696−3717.
(3) Lu, A. H.; Hao, G. P.; Sun, Q.; Zhang, X. Q.; Li, W. C. *Macromol. Chem. Phys.* **2012**, *213*, 1107−1131.
(4) Ryoo, R.; Joo, S. H.; Kruk, M.; Jaroniec, M. *Adv. Mater.* **2001**, *13*, 677−681.
(5) Meng, Y.; Gu, D.; Zhang, F. Q.; Shi, Y. F.; Yang, H. F.; Li, Z.; Yu, C. Z.; Tu, B.; Zhao, D. Y. *Angew. Chem., Int. Ed.* **2005**, *44*, 7053−7059.
(6) Ghanizadeh, G.; Asgari, G. *React. Kinet. Mech. Catal.* **2011**, *102*, 127−142.
(7) Joshi, J. D.; Jabali, V.; Sharma, S.; Patel, C. C.; Patel, A. B. *Asian J. Chem.* **2004**, *2*, 1069−1075.
(8) Liu, T. H.; Li, Y. H.; Du, Q. J.; Sun, J. K.; Jiao, Y. Q.; Yang, G. M.; Wang, Z. H.; Xia, Y. Z.; Zhang, W.; Wang, K. L.; Zhu, H. W.; Wu, D. H. *Colloids Surf., B* **2012**, *90*, 197−203.
(9) http://ntp.niehs.nih.gov/ntp/htdocs/Chem_Background/ExecSumm/MethyleneBlue/MethBlue_exp_toxeffects.html.
(10) Liang, C.; Dai, S.; Guiochon, G. *Anal. Chem.* **2003**, *75*, 4904−4912.
(11) Eltmimi, A. H.; Barron, L.; Rafferty, A.; Hanrahan, J. P.; Fedyanina, O.; Nesterenko, E.; Nesterenko, P. N.; Paull, B. *J. Sep. Sci.* **2010**, *33*, 1231−1243.
(12) He, X.; Zhou, L.; Nesterenko, E. P.; Nesterenko, P. N.; Paull, B.; Omamogho, J. O.; Glennon, J. D.; Luong, J. H. T. *Anal. Chem.* **2012**, *84*, 2351−2357.
(13) Leung, A. C. W.; Hrapovic, S.; Lam, E.; Liu, Y.; Male, K. B.; Mahmoud, K. A.; Luong, J. H. T. *Small* **2011**, *7*, 302−305.
(14) Lam, E.; Leung, A. C. W.; Liu, Y.; Majid, E.; Hrapovic, S.; Male, K. B.; Luong, J. H. T. *ACS Sustainable Chem. Eng.* **2013**, *1*, 278−283.
(15) Tuinstra, F.; Koenig, J. L. *J. Chem. Phys.* **1970**, *53*, 1126−1130.

(16) Maldonado-Hodar, F. J.; Moreno-Castilla, C.; Rivera-Utrilla, J.; Hanzawa, Y.; Yamada, Y. *Langmuir* **2000**, *16*, 4367−4373.
(17) Dresselhaus, M. S.; Jorio, A.; Hofmann, M.; Dresselhaus, G.; Saito, R. *Nano Lett.* **2010**, *10*, 751−758.
(18) Thommes, M. *Chem. Ing. Tech.* **2010**, *82*, 1059−1071.
(19) Gregg, S. J.; Sing, K. S. W. *Adsorption, Surface Area, And Porosity*; Academic Press: London, 1967.
(20) Barrett, E. P.; Joyner, L. G.; Halenda, P. P. *J. Am. Chem. Soc.* **1951**, *73*, 373−380.
(21) AquaSorb 2000-granular coal based activated carbon, Technical Data Sheet, www.jacobi.net.
(22) Langmuir, I. *J. Am. Chem. Soc.* **1918**, *40*, 1361−1403.
(23) Richter, E.; Schutz, W.; Myers, A. L. *Chem. Eng. Sci.* **1989**, *44*, 1609−1616.
(24) Ratkowski, D. A. *Handbook of Nonlinear Regression Models*; Marcel Dekker, New York, 1990.
(25) Radke, C. J.; Prausnitz, J. M. *AIChE J.* **1972**, *18*, 761−768.
(26) Sips, R. *J. Chem. Phys.* **1948**, *16*, 490−495.
(27) Mundhe, K. S.; Gaikwad, A. B.; Torane, R. C; Deshpande, N. R.; Kashalkar, R. V. *J. Chem. Pharm. Res.* **2012**, *4*, 423−436.
(28) Kipling, J. J.; Wilson, R. B. *J. Appl. Chem.* **1960**, *10*, 109−113.
(29) Johnson, C. E., Jr. Methylene blue adsorption and surface area measurements. Paper presented at the *131st National Meeting of the American Chemical Society*; April 7−12, 1957 ; American Chemical Society: Washington, D.C., **1957**,.
(30) Kalousek, M.; Blahnik, R. *Coll. Czech. Chem. Commun.* **1955**, *20*, 782−788.
(31) Los, J. M.; Tompkins, C. K. *J. Chem. Phys.* **1956**, *24*, 630.
(32) Yan, T.G.; Wang, L.J. *BioResources* **2013**, *8*, 4722−4734.
(33) Sharma, P.; Kaur, H.; Sharma, M.; Sahoe, V. *Environ. Monit. Assess.* **2011**, *183*, 151−195.
(34) Foo, K.Y.; Hameed, B.H. *Desalin. Water Treat.* **2010**, *19*, 255−274.
(35) Hubbe, M. A.; Beck, K. R.; O'Neal, WG.; Sharma.. *BioResources* **2012**, *7*, 2592−2687.
(36) Srinivasan, A.; Viraraghavan, T. *J. Environ. Manage.* **2010**, *91*, 1915−1929.
(37) Cigdem, S. O. *Physicochem. Probl. Miner. Process.* **2012**, *48*, 441−454.
(38) Hosseini, S.; Khan, M. A.; Malekbala, M. R.; Cheah, W.; Choong, T.S.Y. *Chem. Eng. J.* **2011**, *171*, 1124−1131.
(39) Mohd-Din, A. T.; B.H. Hameed, B. H.; Ahmad, A. L. *J. Hazard. Mater.* **2009**, *161*, 1522−1529.
(40) Dogan, M.; Ozdemir, Y.; Alkan, M. *Dyes Pigm.* **2007**, *75*, 701−713.
(41) Hosseini, S.; Khan, M. A.; Malekbala, M. R.; Cheah, W.; Choong, T. S. Y. *Chem. Eng. J.* **2011**, *171*, 1124−1131.
(42) Zhu, Y.; Wang, D. Q.; Zhang, X. C.; Qin, H. D. *Fresenius Environ. Bull.* **2009**, *18*, 369−376.
(43) Rahman, M. A.; Ruhul Amin, S. M.; Shafiqul Alam, A. M. *Dhaka Univ. J. Sci.* **2012**, *60*, 185−189.
(44) Berenguer, R.; Marco- Lozar, P.; Quijada, C.; Cazorla- Amoros, D.; Morallon, E. *Energy Fuels* **2010**, *24*, 3366−3372.
(45) Liu, R.-J.; Shen, X.-Q.; Yang, X.-C.; Wang, Q. J.; Yang, F. *J. Nanopart. Res.* **2013**, *15*, 1679.
(46) Joshi, K. M.; Shrivastava, V. S. *Int. J. Nano Dimens.* **2012**, *2* (4), 241−252.